Chapter I.4 Microcoaxial Needle Sensor for Polarographic Measurement of Local O_2 Pressure in the Cellular Range of Living Tissue. Its Construction and Properties

H. Baumgärtl and D.W. Lübbers[1]

1 Introduction

With the progress in polarographic analysis and with the development of various types of needle sensors, in vivo determination of oxygen supply to tissue has become feasible [10–15, 19–21, 23, 43, 56, 57, 68–70, 75, 77]. The smallest types of these polarographic oxygen sensors (POS) have tip diameters of 1–5 μm. Their spatial and temporal resolutions are sufficiently high for satisfactory measurement of intercapillary oxygen partial pressure p_{O_2} [4, 11, 24, 29–32, 40, 49, 52, 67]. However, POS of this size may still cause considerable damage to the tissue. To avoid structural damages and to allow almost punctiform measurements of p_{O_2} in the cellular range, further miniaturizing has been desirable. For this purpose, the techniques and materials used so far have proved insufficient. Aside from poor polarogram characteristics, increasing instability of the measuring signal, sensitivity to mechanical pressure, high residual currents, intolerable drift of calibration curves, reduced stability, as well as insufficient insulation resistance and relatively high ionic sensitivity of the glass shaft of the sensor were observed.

Investigation of the technical details which influence the function of the POS has shown that the measuring properties essentially depend on the quality of the cathode material, chemical composition of the glass, features of the reference electrode, quality of the membrane, and special techniques of treatment. By choice of the proper raw material and suitable techniques – among others vacuum coating – we succeeded in eliminating the main sources of error and have been able to produce a small and reliable needle sensor of mean tip diameter of 0.6 μm, the so-called microcoaxial sensor.

2 Construction of the p_{O_2} Microcoaxial Needle Sensor

Figure 1 shows a schematic drawing of the microcoaxial needle sensor used for polarographic p_{O_2} measurements in the cellular range of living organisms. It is an improved

1 Max-Planck-Institut für Systemphysiologie, Rheinlanddamm 201, D–4600 Dortmund, FRG

Polarographic Oxygen Sensors (ed. by Gnaiger/Forstner)

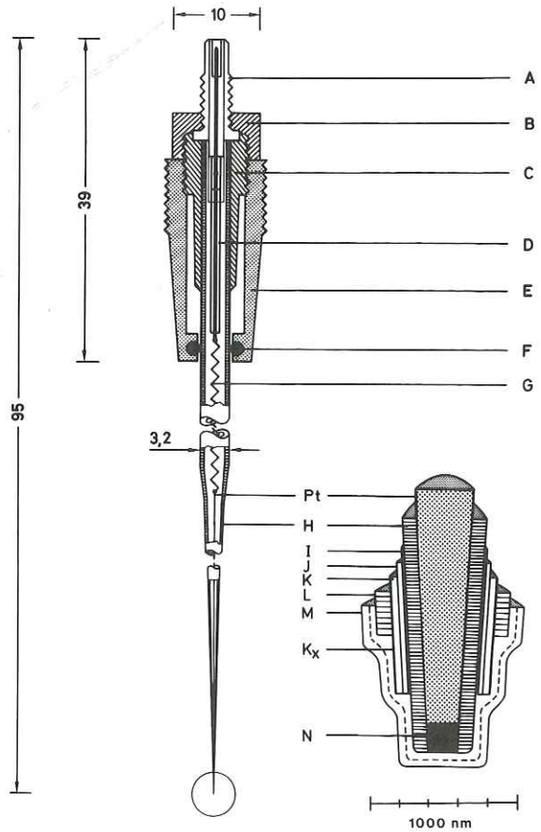

Fig. 1. Schematic drawing of the p_{O_2} microcoaxial needle sensor. *A* chassis socket; *B* nut; *C* metallic contact; *D* polyethylene-coated Cu wire; *E* readily exchangeable Plexiglas housing ground conically and fitting into screw thread; *F* siliconized O-ring; *G* metallic spiral; *H* glass shaft; *I* sputtered Ta-layer, ca. 8 nm; *J* sputtered Pt-layer, ca. 30 nm; *K* sputtered Ag-layer, ca. 62 nm; K_x electrochemically produced AgCl-layer; *L* sputtered dielectric layer such as SiO_2, Al_2O_3, Si_3N_4, Ta_2O_5, $BaTiO_3$; *M* adhesive, nontoxic O_2-permeable double-membrane (collodion, polystyrene, silicone, acrylic-polymere); *N* electrochemically polished cathode surface with recess, electrodeposited gold-layer and electropolymerized membrane [polystyrene or poly-diacetone-acrylamide (PDAA)]

modification of the sensors described by Baumgärtl and Lübbers [13, 14] and Baumgärtl [10] where platinum cathode and reference electrode are situated behind one and the same membrane. The characteristics of this POS are as follows:

1. The active measuring element, the cathode (Pt), is made of a physically or spectrally pure platinum wire (W.C. Heraeus GmbH, D–6450 Hanau) that is 0.2 mm thick and approx. 50 mm long for reasons of mechanical stability. On one end the wire is conically etched down to tip diameters between 0.1 and 0.5 μm over a length of 15–25 mm, using alternating current of controlled voltage.

2. The electrode shaft (H) consists of melting glass free from lead, (GW-Glas, Glaswerk Wertheim, D–6980 Wertheim; or melting glass – 8510, Jenaer Glaswerk Schott & Gen., D–6500 Mainz). The glasses have been selected with regard to their electrical insulation properties, viscosity, wettability, and chemical resistance. Their coefficient of thermal expansion corresponds to that of platinum. Before melting, the glass is thoroughly cleaned in aqueous watery detergent with ultrasound during the organic solvent vapor phase, as well as by heat treatment and ionic bombardment in glow discharge.

3. Under microscopic control the tip of the platinum cathode is fused to the glass capillary (H) over a length of ca. 25 mm with an electrically heated loop. Temperature is continuously controlled. After finishing the tip, the electrode is re-fused in the tip area over about 20 μm with a micro heating loop in order to ensure high stability of the fusion zone platinum/glass and to remove splits and microcracks.

4. Mechanical stability and rigidity, chemical stability and electrical insulation resistance of the glass shaft (H), which is only 100 nm thick in the tip region, are essentially increased by further treatment, such as annealing, chemical heat treatment through ionic exchange in a KNO_3-melt at 350°–400°C, applying electrical tension, ionic bombardment in a glow discharge, or by sputtering thin dielectric layers, such as Ta_2O_5, SiO_2, Al_2O_3, Si_3N_4, $BaTiO_3$, etc. Best results have been obtained with layers of Al_2O_3 or SiO_2, as well as with double layers of Al_2O_3/SiO_2.

5. The form of the electrode tip is determined either by etching and grinding processes or by "pushing" to break off the projecting glass of the tip. The following tip forms are produced: plane (Fig. 1, enlargement of cutout), obliquely ground at an angle of 20°–30° (Fig. 2a) and cone-shaped (Fig. 2b) ones. These procedures result in circular, elliptic, and conic cathode surfaces. In general, the smallest circular cathodes

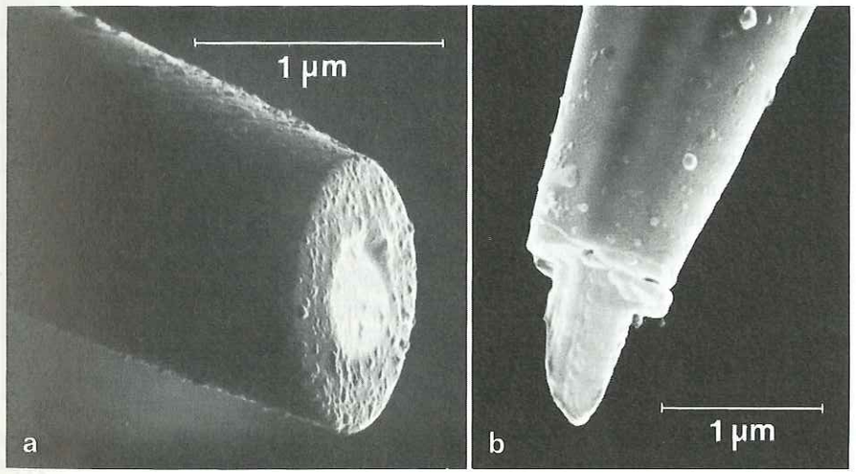

Fig. 2a,b. Scanning electron micrographs of tips of two needle electrodes: a obliquely ground, b etched with hydrofluoric acid

have diameters between 0.2 and 0.5 μm. This corresponds to surfaces of ca. 0.03–0.2 μm^2. In the polarographic circuit the small cathode surfaces produce low O_2 reduction currents ranging from 1×10^{-10} to 2.2×10^{-10} A in air-saturated solutions. The oxygen consumption of the cathodes themselves of 3.5×10^{-7}–7.7×10^{-7} mm^3 O_2/min (= 1.5×10^{-8}–3.4×10^{-8} μmol O_2/min; or 5.0×10^{-7}–1.1×10^{-6} μg O_2/min) is negligibly small and does not essentially influence the p_{O_2} measurements. Under these conditions, the theoretically expected decrease in O_2 pressure of a fluid sample of 1 mm^3 with solubility coefficient $\alpha = 0.01$ (cm^3 O_2/cm^3 atm^{-1}) is ca. 3.6–7.7 Pa/min (= 2.7×10^{-2}–5.8×10^{-2} mm Hg/min). The signal obtained with an obliquely ground electrode tip (angle of 30°) is about 10% higher than that of the plane electrode of identical total diameter. A cathode obliquely ground at 45° augments the signal by about 20%. Cone-shaped cathode surfaces provide an increased signal as well. This is of advantage for measurements requiring an increased signal which is then achieved without increasing the outer diameter of the electrode.

6. A sputtered thin-layer package of Ta/Pt/Ag/AgCl serves as the reference electrode (I-K_x) located at short distance from the tip. It is covered by a thin, sputtered, high-ohmic insulating layer (L) such as to from a small ring. Due to this arrangement, artifacts caused by dc-voltage shifts are rather ineffective. When using rf-sputtering, the very thin metallic reference element is produced with high accuracy. The total thickness of the multicomponent layer is ca. 100 nm (Ta-layer = 8 nm $\triangleq$ 80 Å; Pt-layer = ca. 28 nm; Ag-layer 2 ca. 64 nm). The Ta-layer (I) sticks well to the glass surface, while the intermediate platinum layer (J) guarantees a good electrical conductivity even if the Ag-layer (K) has chlorinated. Usually, a thin AgCl-layer (K_x) develops during routine tests of the measuring properties in the polarographic circuit at ca. –800 mV. The distance of 1–5 μm between platinum cathode and metallic layer serving as the reference anode is produced by etching under the microscope. In addition, the metallic layer is a good electrical shield. The electrical stability of such a reference electrode is excellent.

7. The surface of the platinum cathode may be polluted by foreign metallic influence or abrasives etc. and therefore it is electrochemically polished. The surface condition reached this way favorably influences the measuring properties of the p_{O_2} needle sensor. In some cases, the small recess (N) additionally developing through electropolishing, is also electroplated with a gold layer and thus improves the quality of the cathode surface. Moreover, the recess may be used to reinforce membrane (M) on the cathode and to increase its adhesiveness.

The polarograms of the electrochemically polished platinum cathode and the gold-tipped electrode usually show a clear plateau between –550 and –850 mV and between ca. –500 and –1200 mV, respectively, after intensive rinsing. The electrodeposited gold layer enlarges the cathode surface by its fine granular structure and produces a signal distinctly higher than that of the polished platinum surface. In a p_{O_2} range of 1.3–18.0 kPa (= 10–135 mmHg) the signal drifts ± 9.3% in 30 days with either type. At high O_2 concentration (above 85%) the value is less constant. The small recess (N) can also be filled with fine-spread palladium. This increases the sensitivity to hydrogen so that the sensor is applicable to p_{H_2} measurements after adequate polarization. p_{Cl}-sensors with good selectivity are produced by coating the platinum surface with silver and chlorinating it.

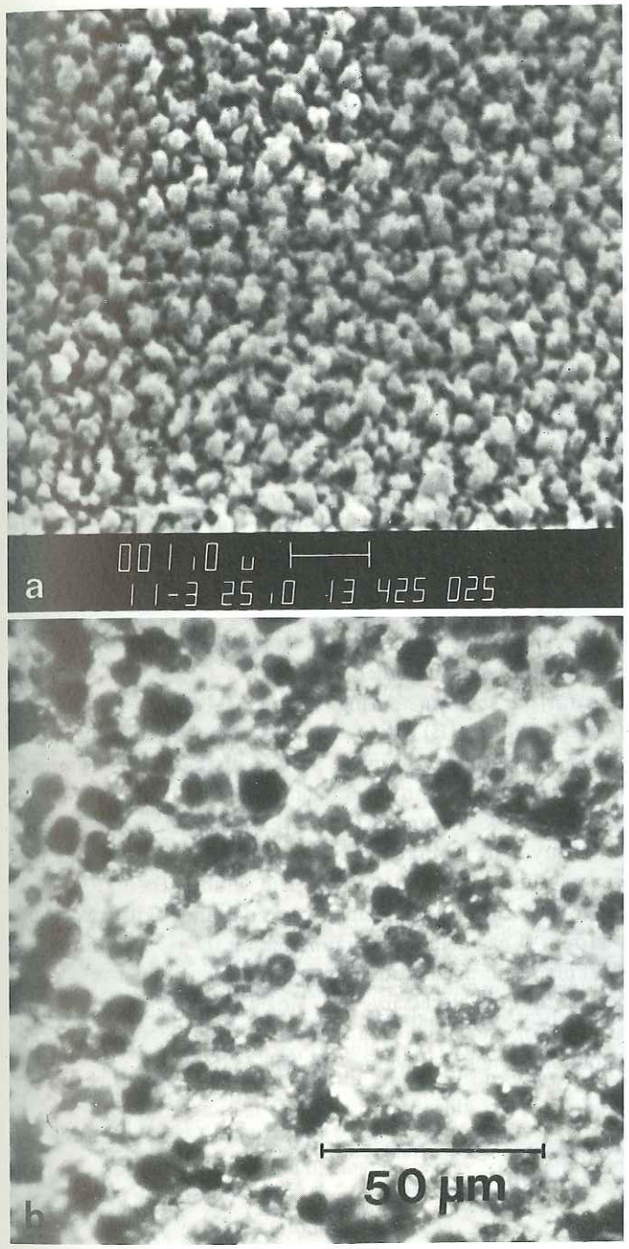

Fig. 3. a Scanning electron micrograph of a polystyrene membrane produced by gas phase polymerization in glow discharge. Nontempered membranes show a coarse-grained structure (size of grain 0.1–0.3 μm), while layers tempered at 200°C are characterized by a fine-grained surface with good sticking properties (bar = 1 μm). **b** Light micrograph of an electropolymerized polydiacetonacrylamid layer (PDAA) on a round, plane macro-Pt cathode

8. The sensor is covered with nontoxic, O_2-permeable membranes (M) made of hydrophilic and hydrophobic materials such as collodion, polystyrene, zapon lacquer, silicone, acrylic polymeres. The filmlike layers are single or multiple, and are produced either in a dipping process or by electropolymerization or by gas phase polymerization in glow discharge (Fig. 3a,b); they adhere to cathode and anode. They produce a defined diffusion field in front of the sensor. This is necessary for absolute p_{O_2} measurements; only a defined p_{O_2} field allows p_{O_2} calibration of the POS. The membrane thickness of our POS approximately corresponds to the dimension of the cathode diameter. For a double membrane of collodion and polystyrene, the diffusion error is $< 5\%$ and the response time 1–3 s. In most cases, this is sufficient to measure the kinetics of the p_{O_2} field. The quality of the membrane must be controlled in a special test.

9. The tip diameter of the p_{O_2} microcoaxial sensor, visualized under the scanning electron microscope, is about 0.6 μm when measured about 0.2 μm from the extreme tip, while the diameter of the platinum cathode, the glass shaft and the membrane each account for about 0.2 μm (see enlargement in Fig. 1). At 1–5 μm from the tip the thin-layer reference element (I-K_x) thickens the sensor for another 0.2 μm. A total diameter of about 15 μm is measured about 150 μm from the tip. Due to these dimensions, compression of the vessels is avoided in most cases. Neither microcirculation nor O_2 diffusion are influenced so that almost punctiform measurements are feasible. Further improvement is attained with optimum membranization as achieved by electropolymerization. With this technique the surface is membranized without appreciably thickening the electrode shaft. The diameter of the POS is reduced by about 0.2 μm and so an actual diameter of 0.3–0.4 μm is obtained.

10. A connecting system for the small measuring current (A-G) protected against wetness also serves as the sensor housing (E) with ground and screw thread and makes the sensor handy and easy to exchange by a simple plug (A,C,D,G). The complete POS is sterilizable and may also be used for chronic implantations.

The production of this type of POS requires a relatively high technical investment in a specially equipped laboratory. The laboratory is under slight excess pressure and can only be entered via several dust-binding mats (Unichem GmbH, D–6000 Frankfurt 90). Here, three Laminar-flow clean work benches are combined with two clean work cabins with vertical current (Ceag-Schirp-Reinraumtechnik, D–4714 Selm-Bork) in such a way that the critical phases of production can be carried out under the conditions of extreme cleanliness absolutely necessary. The single steps in producing the p_{O_2} [9] microcoaxial needle sensor are shown as a schematic block picture in Fig. 4. A detailed description of production methods will be published elsewhere.

3 Test of Function and Measuring Properties of p_{O_2} Microcoaxial Needle Sensor

3.1 Performance of Bare Electrodes

3.1.1 p_{O_2} Signal of Platinum Cathode

The quality of a p_{O_2} electrode is, apart from the melting process which determines the boundary platinum/glass, mainly influenced by the surface condition of the cathode.

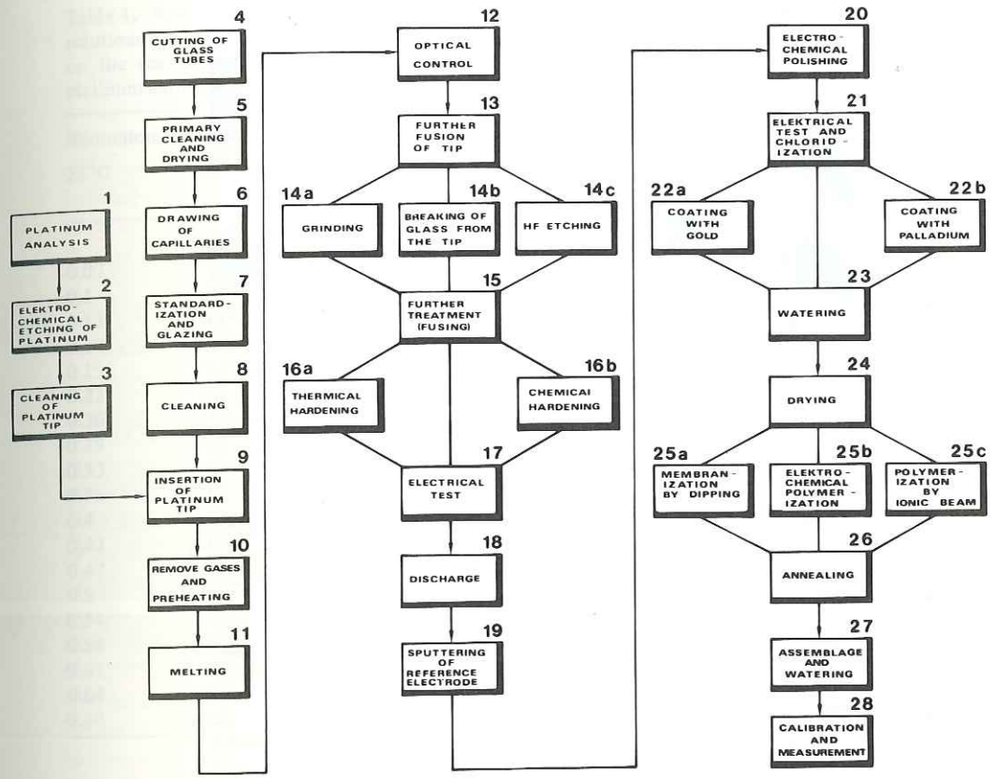

Fig. 4. Schematic drawing of the single steps necessary for producing the p_{O_2} microcoaxial needle sensor

Experience has shown that high cleanliness of the surface and the purity of the platinum used are of extreme importance. Tests in the polarographic measuring circuit have shown that the surface condition is favorably influenced by electrochemical polishing of the Pt-cathode. Figure 5 shows an original registration of the O_2 reduction currents of three needle sensors in an unpolished (I) and electrochemically polished (II) condition. In an untreated condition the three sensors show continuously increasing signals, whereby sensors a and b exhibit an especially unsteady behavior. After electropolishing the same sensors in diluted KCN-solution with ac current, the reproduceability of the signal was improved, the unsteadiness was essentially diminished, and the drift was reduced to a minimum. An effect of electropolishing was observed in 95% of sensors. Only in a few cases was re-etching necessary.

Apart from a clean cathode surface, electropolishing produces a small recess, the size of which is assessed by determining the so-called stirring effect R_e (diffusion error). The stirring effect is determined under defined convection conditions and is calculated according to formula

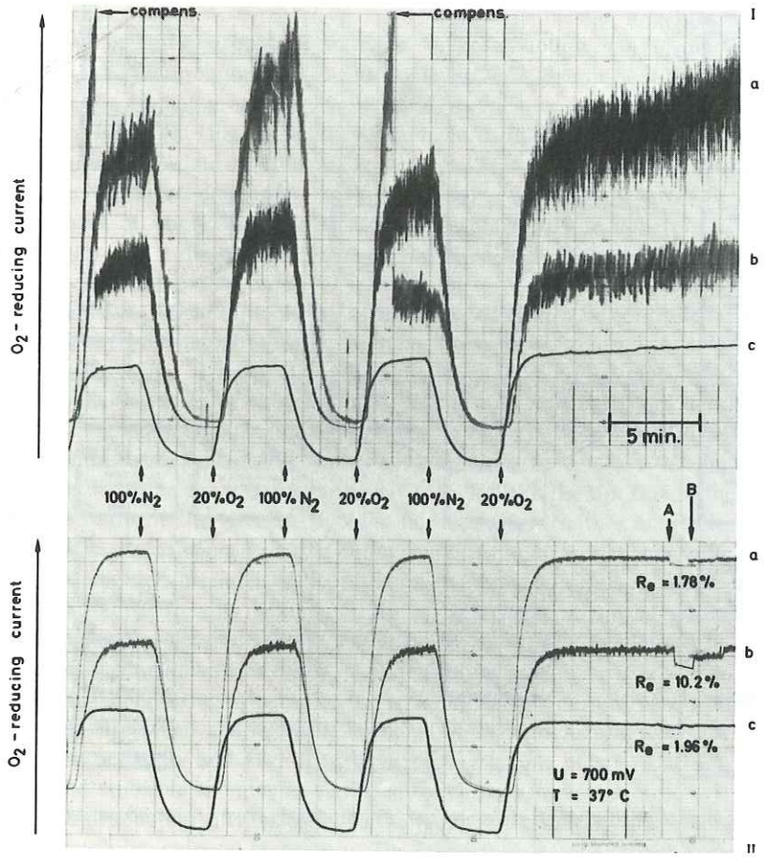

Fig. 5. Behavior of nontreated (I) and electrochemically polished (II) platinum needle sensors. The signals of unpolished sensors (*a, b, c*), recorded in Theorell buffer solution (pH = 7.2) at continual change of calibration gas steadily increase, whereby sensors a and b show considerable unrest. After polishing with ac current in dilute KCN solution, the reproduceability of the signal improves, the high amplitude essentially diminishes and the drift is eliminated. The small stirring effects (R_e) of sensors *a* and *c* indicate recesses greater than that of *b*. *A* stop of gas supply (unstirred medium), *B* switching on gas supply (stirred medium)

$$R_e = \frac{I - I_1}{I} \times 100\% \text{ or } (1 - \frac{I_1}{I}) \times 100\%, \quad (1)$$

where I is the p_{O_2} signal produced in stirred solution and I_1, the p_{O_2} signal in unstirred solution.

A low R_e value suggests a big recess and means that the O_2 particle flow is mainly restricted to the interior of the recess [see Eq. (4) with large z]. Figure 5 shows a big recess in curve a (R_e = 1.78%) and curve c (R_e = 1.96%) and a smaller one in curve b (R_e = 10.2%).

Table 1. Reduction current I_1 in H_2O and diluted aqueous solutions (25°C and 37°C) at air saturation in dependence on the size of platinum cathode surface. r_o = radius of platinum cathode, A = surface area of platinum cathode

Reduction current (nA)		Dimension of cathode	
25°C	37°C	r_o (μm)	A (μm^2)
–	0.04	0.05	0.008
0.07	0.09	0.1	0.031
0.1	0.13	0.15	0.071
0.13	0.18	0.2	0.126
0.16	0.22	0.25	0.196
0.19	0.27	0.3	0.283
0.22	0.32	0.35	0.385
0.26	0.36	0.4	0.503
0.29	0.4	0.45	0.636
0.33	0.45	0.5	0.785
0.36	0.5	0.55	0.950
0.4	0.55	0.6	1.131
0.43	0.6	0.65	1.327
0.47	0.64	0.7	1.539
0.5	0.69	0.75	1.767
0.54	0.74	0.8	2.011
0.58	0.78	0.85	2.270
0.61	0.83	0.9	2.545
0.64	0.89	0.95	2.835
0.68	0.95	1.0	3.141

Under conditions in other respects constant, the O_2 reduction current depends on the size of the cathode surface and so this parameter provides information about the platinum surface of the needle electrode. Table 1 shows the data obtained from measurements on bigger and exactly defined platinum surfaces extrapolated to thin cathode diameters. In general, the O_2 reduction currents of our smallest needle electrodes amount to 0.06–0.25 nA in air-saturated, diluted electrolytes (such as 0.1 mol dm^{-3} KCl, NaCl etc.) at 37°C, which corresponds to cathode diameters of 0.15–0.5 μm. This has been confirmed with control measurements made under the scanning electron microscope.

3.1.2 p_{O_2} Signal of the Gold Cathode

In comparison to platinum as a cathode material, gold has a broader plateau in the polarographic measuring circuit. This has the advantage that with p_{O_2} measurements in vivo in various tissues, the effective polarization current is not influenced by small biological dc fluctuations. We prefer electrodeposition of Au on the Pt-cathode surface, as it is extremely difficult to seal thin tips of gold wire into glass because no glass available matches the coefficient for thermal expansion. Satisfactory layers must be

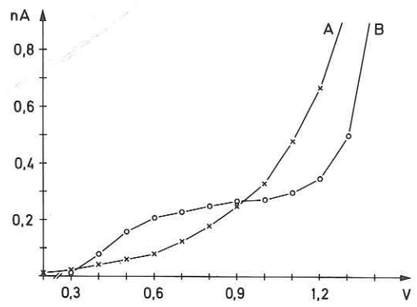

Fig. 6. Polarogram of a gold-plated p_{O_2} microcoaxial needle sensor recorded immediately after gold-plating (*A*) and after intensive soaking for 10 days (*B*). The broad polarogram typical for gold running almost in parallel with the abscissa, is distinct only in curve *B*

very thin and require careful cleaning in bidistilled water. The best measuring properties of galvanically gold-plated electrode tips were seen after watering for 10days.

Figure 6 shows a polarogram of a galvanically gold-plated microcoaxial needle sensor with a layer thickness of about 1 μm. Polarogram (A) was recorded immediately after galvanizing and (B) after 10 days of thorough cleaning by watering. The broad plateau seen in curve B reaches from 600 to 1100 mV which is typical for gold. Gold-plated needle sensors usually have a higher signal, because the fine-grained surface structure enlarges the cathode surface. According to information received from MRC (Materials Research Corporation, Orangeburg/New York), platinum even of the highest degree of purity produceable contains, aside from dissolved gases (14.5 ppm of H_2, O_2, N_2), impurities such as 17.5 ppm nonmetal (C, S), 30 ppm Fe, 15 ppm Rh, 7 ppm Al, 5 ppm W, 2.5 ppm Cr, Ni, Ti, Zr each. It cannot be excluded that some of these impurities unfavorably influence the p_{O_2} measurements. For some applications we therefore use the galvanic Au-layer for further improvement of the platinum micro electrodes.

3.1.3 Insulation Resistance and Ionic Sensitivity of Thin Glass Electrode Shaft

Routine control has shown that the quality of electrical insulation is recognizable from the size of the current in N_2 saturated solution, I_r.

This current should be very low. The ratio I_{air}/I_r is high if

1. the Pt-cathode is especially well fused to the glass,
2. the glass has a high electric insulation resistance and
3. the thin glass wall has not been damaged by microcracks.

In general, a mean quotient of 35 (max: $>$ 100; n = 923) is reached with GW-glasses. POS with a quotient $<$ 5 should not be used for p_{O_2} measurements. Such sensors usually have microcracks and splits between platinum and glass wall. In most cases, they also have long response times.

Apart from GW-glass, the lead-free soft glass 8510 has been used for the glass shaft of the sensor. Its coefficient of thermal expansion is about 9.3×10^{-6} in the range

20°–300°C. Its insulation resistance (t_K = 322) is especially high, and during fusing in it forms very thin and mechanically stable insulation layers on the platinum wire. As compared with other melting glasses, this glass shows little sensitivity to K^+ and Na^+ ions. Layers of untreated and thin GW-glass of 0.1 μm may have a pH sensitivity of 16–20 mV/pH. The ionic sensitivity is strongly decreased by a layer of Si_3N_4 sputtered onto the glass shaft and by the metallic thin-layer package mentioned above, which is used as the reference electrode. Though lead glasses are superior because of their high insulation resistance, they cannot be used for sealing platinum cathodes because their chemical resistance in aqueous solutions is so low that Pb is released.

3.2 Performance of Membranized Sensor

3.2.1 Effect of the Membrane on the O_2 Diffusion Field in Front of the Platinum Cathode

With polarographic p_{O_2} measurement, oxygen molecules are reduced on the cathode surface. In the neutral and alkaline ranges the chemical reaction is as follows:

$$O_2 + 2\,H_2O + 4\,e^- = 4\,OH^-. \qquad (2)$$

Electrochemical reduction generates the signal in the polarographic circuit. Since the cathode continuously consumes oxygen, a continuous flux of oxygen molecules toward the electrode develops. Under the assumption that at optimum polarization all of the oxygen molecules are immediately reduced, the number of oxygen molecules on the cathode surface and, hence, p_{O_2} are zero. With this boundary condition, the p_{O_2} in the diffusion field developing in front of the electrode has been calculated. The calculation provides information about the catchment range of the electrode [28, 29, 65]. Using cylindrical coordinates, the stationary state of the O_2 diffusion field of the plane and circular electrode is described by

$$p\,(r_E,z) = p_{O_2}\,(1 - \tfrac{2}{\pi}) \int_0^\infty \frac{\sin\,(\lambda r_o)}{\lambda}\, J_o\,(r_E\lambda)\exp\,(-\lambda z)\mathrm{d}\lambda, \qquad (3)$$

where $p(r_E,z)$ is p_{O_2} in the diffusion field
p_{O_2} true p_{O_2} of medium, uninfluenced by O_2 diffusion field
r_o radius of cathode
r_E horizontal distance from the centre of electrode
z vertical distance from that plane
J_o zero order Bessel function
λ integration variable

(for solutions of Eq. (3) see [28]).

Figure 7 shows the p_{O_2} distribution calculated for three different sites (r_E = 0.73 mm, 0.6 mm, 0.01 mm) of the bare, circular cathode surface (r_o = 0.75 mm). Percentage p_{O_2} is plotted on the ordinate and distance (z) from the cathode surface in mm, on the abscissa. The zero point on the abscissa indicates the cathode surface where p_{O_2} is zero. We see that the diffusion field of a bare electrode in any case

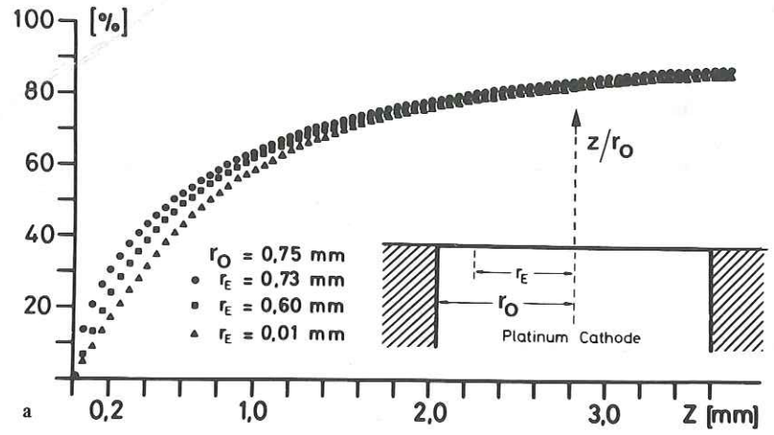

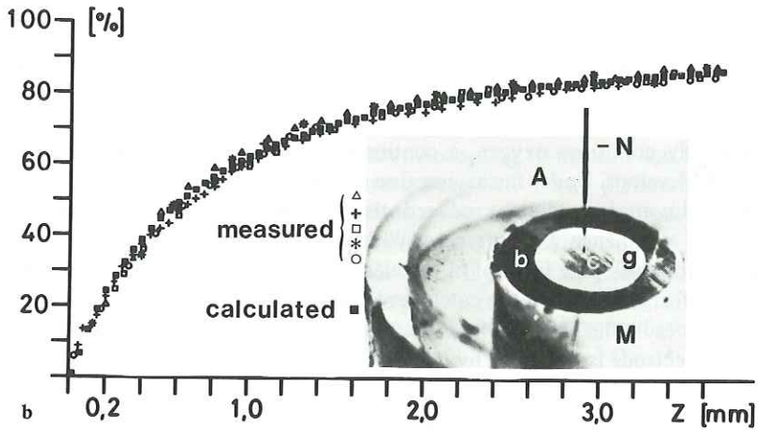

Fig. 7. a Calculated p_{O_2} distributions in the stationary diffusion field of a plane, circular cathode surface (r_0 = 0.75 mm) for three different horizontal distances from the center of the electrode (r_E = 0.73 mm, 0.6 mm, 0.01 mm). *Ordinate:* percentage p_{O_2} of true tissue p_{O_2} of medium, *abscissa:* distance (z) from cathode surface. The zero point on the abscissa indicates the cathode surface where p_{O_2} is zero. With a bare electrode, the diffusion field spreads far into the medium to be measured. 3 mm (≙ 4 r_0) distant from the cathode surface, p_{O_2} is about 85% of the true p_{O_2} of the medium. The p_{O_2} distribution is different at different sites. In the center of the cathode, its course is flatter than at the periphery, since the flow density increases toward the border of the cathode. **b** Comparison between measured and calculated p_{O_2} distribution in the diffusion field of a circular Pt-cathode (c) (r_0 = 0.75 mm) for a horizontal distance from the electrode, r_E = 0.6 mm. With a macro POS, *M* (c plane, circular Pt cathode of 1.5 mm diameter, g glass insulation, b ring-shaped Ag/AgCl reference electrode) a diffusion field is produced in a defined agarose layer, *A* (d 13.0 mm; z 6 mm). The p_{O_2} distribution satisfactorily agrees with the calculated p_{O_2} course, as measured with a microneedle sensor, *N*, by advancing it continuously from the agarose layer toward the macro POS

spreads asymptotically with increasing distance from the cathode surface, reaching far into the medium to be measured. When defining the catchment range of an electrode as being that area which supplies 90% of the oxygen to the electrode, the approximate value is $z_{90} = 6.3\ r_0$. Accordingly, in our example, the distance of the z_{90} plane from the plane circular electrode is 4.7 mm, which implies that up to this distance from the cathode surface, the electrode current is influenced by disturbances of the O_2 diffusion field, e.g., by convection or changes of the diffusive properties of the medium. Because of the particularly large catchment range of the bare electrode, such electrodes mostly do not develop a constant diffusion field in front of the platinum wire and therefore are not applicable to absolute p_{O_2} measurements in the tissue. With an ideal membrane the O_2 permeability, P_m of which is very small as compared to that of the sample medium, P_s the p_{O_2} decrease would be entirely restricted to the membrane. In practice, however, the diffusion field, i.e., the p_{O_2} decrease, always begins in the medium. The effect of a p_{O_2} decrease in the medium can be shown by stirring. The difference in the reduction current between stirred and unstirred medium of a membranized electrode directly indicates the diffusion error, i.e., the difference between true p_{O_2} of the medium (stirred) and p_{O_2} which is falsified by the O_2 diffusion within the medium (unstirred). Therefore the stirring effect can be used to test the POS.

The p_{O_2} distribution determined theoretically in the stationary diffusion field of a bare electrode has been experimentally confirmed [11, 13]. The result of such an experiment is shown in Fig. 7b. In that case, an O_2 diffusion field was produced with a macro POS, M, in an agarose layer, A, superimposing the sensor. The p_{O_2} distribution thus produced was measured with a membranized needle sensor, N. Comparison of the measured values (out of five experiments) with the calculated p_{O_2} distributions shows a very good agreement which substantiates the validity of the model mentioned above. Apart from the fact that all of the oxygen molecules are immediately reduced on the cathode surface and so p_{O_2} on the cathode surface is zero, the experiments show that the spatial resolution, i.e., the catchment range, of our micro needle sensor is small enough to allow absolute – almost punctiform – p_{O_2} measurements.

3.2.2 Control of the Membrane

Exact p_{O_2} measurements require covering of the electrode with a membrane which is homogeneous, pinhole-free, adhesive, nontoxic, gas-permeable and water-resistant. The p_{O_2} can be clearly related to the O_2 reduction current only if such a membrane determines the O_2 diffusion toward the electrode. Not being visible on our small needle sensors, the membranes are not optically measurable, and so indirect methods such as determination of the stirring effect must be used.

With the aid of the stirring effect the signal difference between stirred and unstirred solutions is described. According to [28, 29], the stirring effect (diffusion error) for a membranized sensor is:

$$R_e = \frac{1}{1+\delta} \times 100\% \quad \text{with} \quad \delta = \frac{P_s}{P_m} \times \frac{z_m}{r_o}. \tag{4}$$

Table 2. Stirring effect (R_c) in dependence on membrane thickness and radius of cathode (z_m/r_o) under different permeability coefficients (medium/membrane = P_s/P_m). The stirring effect becomes smaller (1) with increasing thickness of membrane, (2) with increasing ratios of permeability, (3) with decreasing radius of the cathode. According to the values reported for oxygen permeability (37°C) in the literature (see Table 3), the ratios for permeability P_s/P_m of an electrode covered with a collodion membrane ($P_m = 1.49 \times 10^{-12}$ mol O_2 cm^{-1} s^{-1} $atm^{-1} \triangleq 1.47 \times 10^{-14}$ mol O_2 cm^{-1} s^{-1} kPa^{-1}) are: 23.5 in water (with $P_s = 3.5 \times 10^{-11}$ mol O_2 cm^{-1} s^{-1} $atm^{-1} \triangleq 3.45 \times 10^{-13}$ mol O_2 cm^{-1} s^{-1} kPa^{-1}); 13.5 in brain cortex (with $P_s = 2.01 \times 10^{-11}$ mol O_2 cm^{-1} s^{-1} $atm^{-1} \triangleq 1.98 \times 10^{-13}$ mol O_2 cm^{-1} s^{-1} kPa^{-1}); 12.5 in lung tissue (with $P_s = 1.86 \times 10^{-11}$ mol O_2 cm^{-1} s^{-1} $atm^{-1} \triangleq 1.82 \times 10^{-13}$ mol O_2 cm^{-1} s^{-1} kPa^{-1}); 12.2 in heart muscle (with $P_s = 1.82 \times 10^{-11}$ mol O_2 cm^{-1} s^{-1} $atm^{-1} \triangleq 1.81 \times 10^{-13}$ mol O_2 cm^{-1} s^{-1} kPa^{-1}); 4.0 in 30% protein solution (with $P_s = 5.95 \times 10^{-12}$ mol O_2 cm^{-1} s^{-1} $atm^{-1} \triangleq 5.87 \times 10^{-14}$ mol O_2 cm^{-1} s^{-1} kPa^{-1}). To obtain a stirring effect lower than 5% e.g. when measuring p_{O_2} in brain tissue, the membrane thickness should be 1.5 times the cathode radius

z_m/r_o	$P_s/P_m = 1$	$P_s/P_m = 2$	$P_s/P_m = 5$	$P_s/P_m = 10$	$P_s/P_m = 15$	$P_s/P_m = 20$	$P_s/P_m = 25$
0.1	90.9	83.3	66.7	50.0	40.0	33.3	28.6
0.5	66.7	50.0	28.6	16.7	11.8	9.1	7.4
1.0	50.0	33.3	16.7	9.1	6.2	4.8	3.8
1.5	40.0	25.0	11.8	6.3	4.3	3.2	2.6
2.0	33.3	20.0	9.1	4.8	3.2	2.4	2.0
2.5	28.6	16.7	7.4	3.8	2.6	2.0	1.6
3.0	25.0	14.3	6.3	3.2	2.2	1.6	1.3
3.5	22.2	12.5	5.4	2.8	1.9	1.4	1.1
4.0	20.0	11.1	4.8	2.4	1.6	1.2	1.0
4.5	18.2	10.0	4.3	2.2	1.5	1.1	0.9
5.0	16.7	9.1	3.8	2.0	1.3	1.0	0.8

Here $P_s = S_s \times D_s$ is the permeability coefficient (Chap. I.3) of oxygen in the sample medium where S_s is the solubility coefficient and D_s the diffusion coefficient (see Tables 2 and 3), P_m is the permeability coefficient of oxygen in the membrane (see Table 2 and Chap. I.1), z_m is the thickness of the membrane, and r_o the radius of the cathode.

Accordingly, diminishing with increasing δ, a small stirring effect is achieved if (1) the ratio of the permeability coefficients P_s/P_m is great, (2) the membrane is thick, (3) the radius of the electrode is small. Table 2 shows the stirring effect in dependence on the membrane thickness under various conditions of diffusion permeability. It follows from Eq. (4) that an insufficient membrane (small z_m, P_m close to P_s) produces a large stirring effect.

However, there may be cases where determination of the stirring effect is not sufficient and so an additional test becomes necessary. Since significant differences exist between bare and membranized electrodes in different solutions, the difference can be used to determine quickly and reliably the quality of a membrane. The p_{O_2} signal of POS with unsatisfactory membranes continuously decreases down to insensitivity to oxygen in calibration solutions containing Ca^{2+} and Mg^{2+} as cations and phosphate, carbonate and/or sulfate as anions. In contrast, optimally membranized sensors show stable measuring properties in the presence of these critical ions. A bicarbonate buffer (pH = 7.4) of the following composition has proved to be a good test solution:

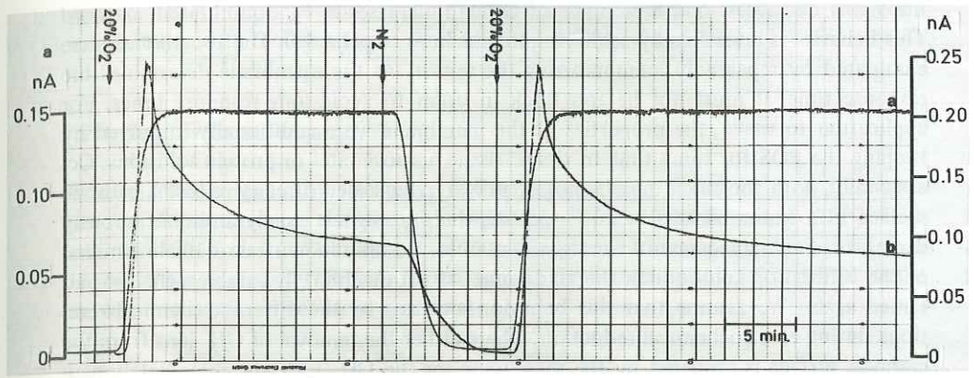

Fig. 8. p_{O_2} signals of (*a*) an optimally membranized and (*b*) a bare or too thinly membranized needle sensor in CO_2-bubbled Ringer solution containing calcium and magnesium (37°C). The signals of needle sensors with defect or too thin membranes drift considerably to low values and may sink down to O_2-insensitivity when kept in this solution for some time. In addition, when changing the calibration gas from N_2 to O_2, the signal shows an overshoot. Changing calibration gas from O_2 to N_2 results in a two-phase course of the signal. Optimally membranized sensors are superior due to stable measuring behavior

26 mmol dm^{-3} $NaHCO_3$, 2.6 mmol dm^{-3} $CaCl_2 \times 2\,H_2O$, 10 mmol dm^{-3} glucose, 124 mmol dm^{-3} NaCl, 4.9 mmol dm^{-3} KCl, 1.3 mmol dm^{-3} KH_2PO_4 and 1.3 mmol dm^{-3} $MgSO_4 \times 7\,H_2O$.

Figure 8 shows an example of an original registration. The p_{O_2} signal of sensor a having an intact membrane always returns to initial values after change of the calibration gas, whereas the O_2 reduction current of sensor b having a defect membrane continuously decreases and, in addition, strongly overshoots in CO_2-bubbled bicarbonate solution when changing from N_2 to air. At change from air to N_2, in most cases the curves of the insufficiently membranized POS show a two-phase course in that test solution (see sensor b). We have not yet investigated which chemical reactions are responsible for this behavior. We assume that insoluble compounds of Ca^{2+} and Mg^{2+} with hydroxides, phosphates, carbonates, and sulfates are formed and precipitate on the defect membrane and perhaps on the bare platinum surface. As a consequence, the diffusion path for O_2 increases continuously, the precipitate also changes the surface conditions of the platinum cathodes and thus, the p_{O_2} signal decreases. This has been substantiated by the fact that the measuring properties of such POS are almost completely normalized by dissolving the precipitates of hydroxide, phosphate, and carbonate by acidification of the calibration medium to pH of approx. 4.5. Here it should be mentioned that salts of carbonate, sulfate, and phosphate, which do not form precipitates, do not affect the polarographic behavior of the platinum cathode.

Organic sulfur compounds especially influence imcompletely membranized sensors. We added 16 mg of cystein to a 200 cm^3 magnesium-phosphate calibration solution and observed extreme changes in the signal. While an optimally membranized sensor scarcely perceives a deviation of the signal, with incompletely membranized sensors

the signal decreases in the presence of O_2 and increases in N_2-equilibrated solution. This behavior is reversible by acidifying the medium to pH = 4.0. The above effects are eliminated by repeatedly membranizing the sensor. As the membrane determines the response time, it must not be too thick in order to avoid long response times. For application to tissue, the properties of the membrane were additionally improved by keeping the POS for some time in tissue, tissue homogenates or protein solutions. Occasionally, with too-thick membranes of polystyrene sealed directly onto the cathode surface in a sinter process at 200°–250°C, the p_{O_2} signals slowly and continuously decreased. Such a decrease of the signal was observed only in neutral or alkaline milieu of the calibration solution. In the acid range, at pH of about 4, a stable signal was attained again. We assume that this behavior is caused by the different chemical reactions during electrochemical reduction, where either the removal of OH^- ions from the cathode surface is hindered by the membrane, or the OH^- ions are immediately neutralized to water by H^+ ions.

3.2.3 Response Time

The time needed by the POS to reach 90% of the new gas pressure value after a sudden change in gas pressure, is called response time, τ_{90}:

$$\tau_{90} \cong c \frac{z_m^2}{D_m} , \tag{5}$$

where z_m is thickness of membrane; D_m, diffusion coefficient of membrane; c, a constant ([28, 30] Chap. I.1).

The response time can be kept short if the membrane is easily diffusible and its thickness is low. As mentioned above, the membrane characteristics determine the stirring effect as well. Both parameters appear as systematic errors. Since they behave contrarily, a sensible compromise must be made by choosing the proper membrane:

1. a thick membrane for a small stirring effect, and a thin membrane for a short response time. However, the membrane must still be thick enough to prevent the O_2 signal from overshooting;
2. a low diffusion conductivity for a small stirring effect, and a high diffusion coefficient for a short response time.

In practice it is very difficult to fulfill all of these conditions at the same time. It has to be taken into account that the membrane thickness influences the response time quadratically, the stirring effect linearly. A material suitable for a good membrane should have a high O_2 diffusion coefficient, but a small solubility for O_2. So far, various materials have been used, such as collodion [13, 22, 77], polystyrene [8, 12, 68], zapon lacquer [13] as well as other film-forming polymeres [15, 34, 69]. We measured 90% response times of 1–3 s with membranes of collodion, polystyrene, and cellulose derivates whose thicknesses approximately corresponded to the diameter of the cathode. Hydron membranes (Hydron-Polymer Type XE-3, Hydron Laboratories Inc., New Brunswick, N.J. 08902) made of polyhydroxyethylmethaceylates show an interesting

behavior. Their response time is short when the stirring effect is reduced. The good compatibility with biological tissue is another advantage of hydron.

3.2.4 Sensitivity to Temperature

We tested the temperature sensitivity in the range between 1° and 50°C on 36 sensors and found that the mean changes in the signal per °C were 2.1% from 15°–25°C, 2.3% from 25°–35°C and 2.7% from 35°–45°C. The temperature sensitivities of different sensors differ immensely. Precise measurements require calibration of each POS at the temperature of the object to be measured.

3.2.5 Sensitivity to Light

At certain wavelengths the microcoaxial needle sensor shows sensitivity to light and reacts with an increase in the signal. In some special calibration experimensts we illuminated the shaft of the sensors laterally with a microscopic lamp (Osram 6 V/15 W with heat filter) in Theorell buffer solution (pH = 7.2) and found an immediate increase in the signal by about 1.4%. As soon as illumination was interrupted, the signal decreased to its initial value. At re-illumination, the signal increased again by the same amount. Illumination of the same sensor with light guides (type KL 150 B, Schott/Mainz) did not change the signal.

3.2.6 Stability and Drift of the Signal

For each POS the signal is different and can change with time. We investigated the stability of the signals of seven microcoaxial needle sensors (0.1–0.15 nA) in air-saturated Theorell buffer solution at 37°C over a period of 30 days. During this period we observed a change of ± 9.3% in the air value. The change of the zero point (in nitrogen) was only ± 1.3%. It was interesting that the most constant values were measured between the 11th and 23rd day (during this period the stability of the polarogram was also best).

3.3 Accuracy of Calibration and Measurement of Needle Sensors

To allow an exact quantitative p_{O_2} measurement, needle sensors should be calibrated in a solution whose diffusion conductivity for O_2 resembles that of the medium to be measured. We calibrate in a glass vessel placed in a Faraday cage. The vessel made of highly insulating laboratory glass is earthed by a calomel electrode. Temperature is continuously monitored by a thermosensor. Four sensors can be calibrated at the same time. For reasons of accuracy, calibration curves should be measured in the p_{O_2} range in which the measurements are to be made. Figure 9 shows that linear calibration curves are obtained in both high (A) and low (B) p_{O_2} ranges.

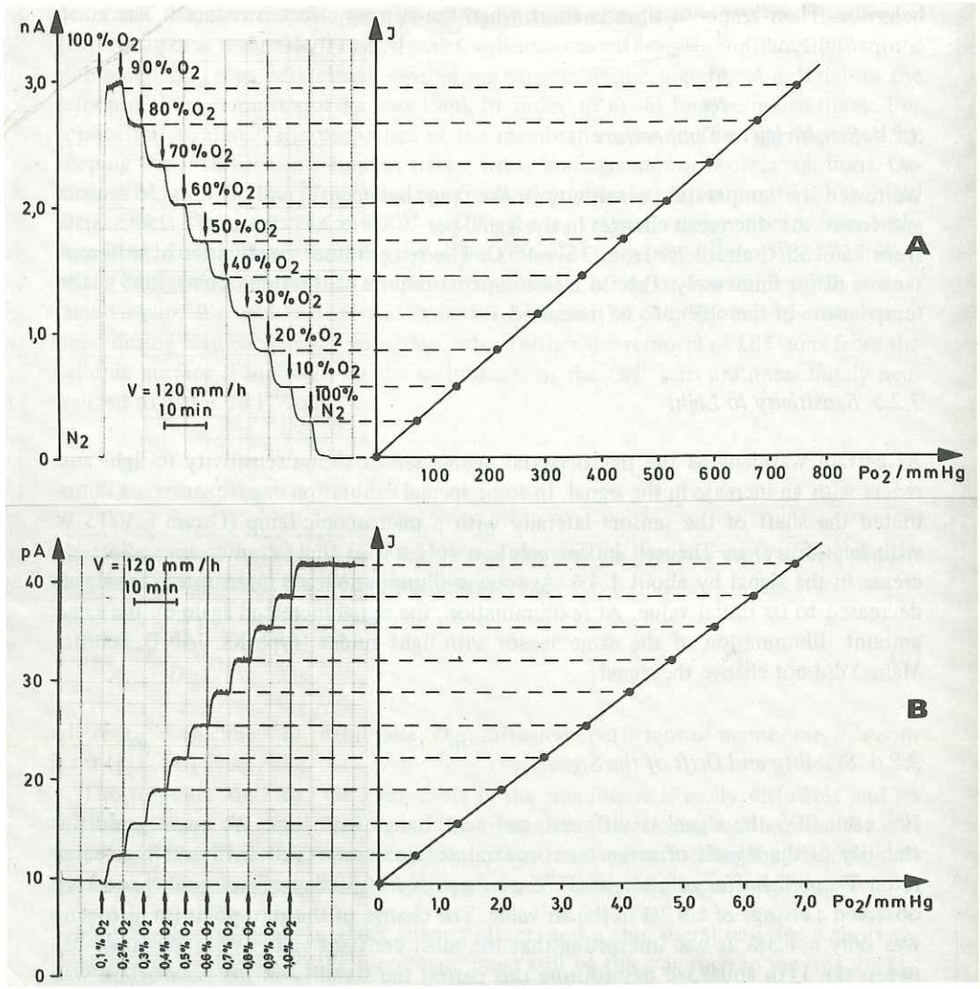

Fig. 9A,B. Calibration curves of a p_{O_2} microcoaxial needle sensor at high (A 0–760 mmHg $\triangleq$ 0–101 kPa) and low (B 0–7 mmHg $\triangleq$ 0–0.9 kPa) p_{O_2} ranges. The two original registrations show 11 spot calibrations in Theorell buffer (pH = 7.2) at 37°C. Plotting reduction current (*ordinate*) versus O_2 partial pressure (*abscissa*) results in linear calibration curves in both pressure ranges

Fig. 10a. Comparison of the p_{O_2} signals to be theoretically expected (– • –) with those actually recorded (– * –) using bare platinum cathodes with circular surfaces (r_0 = 10 μm) in different biological media (37°C). *Dotted area* indicates the size of the signals to be theoretically expected in water. The experimentally determined values for both water and diluted aqueous solutions are within these boundaries. When relating the p_{O_2} values measured in tissue to the calibration curve recorded in diluted electrolyte solution, considerable errors of measurement may arise if either bare electrodes or POS with defective membranes were used. These errors are due to the different diffusive properties. The absolute values determined may be too low: in brain by a factor of 1.4, in the lungs of 1.5, in heart of 1.7, in muscle of 2.6, and in connective tissue of 3.2

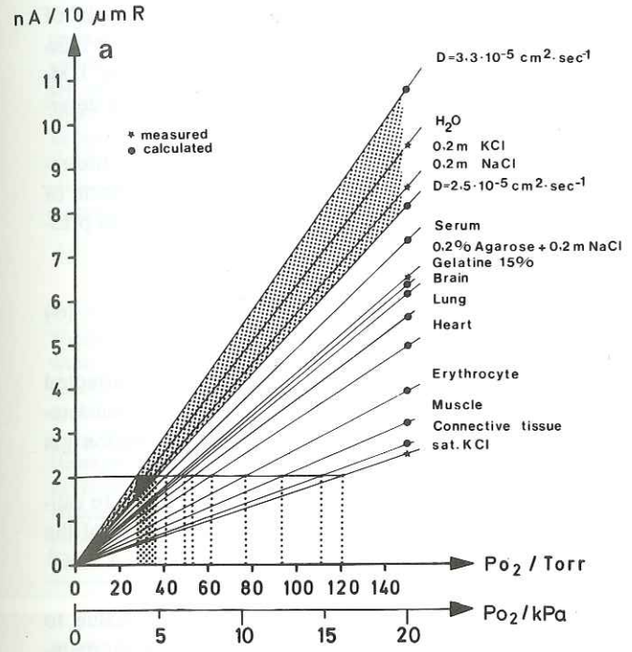

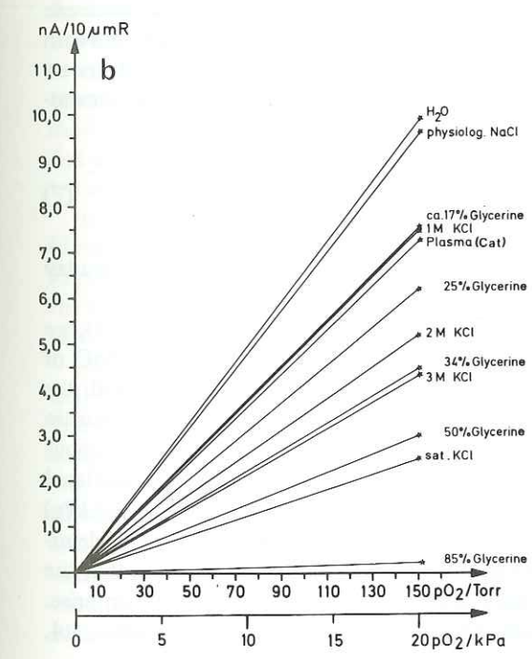

Fig. 10b. p_{O_2} signals experimentally determined for a bare platinum electrode with circular surface (r_0 = 10 μm) in media of different concentrations (37°C). Calibration errors can be minimized by adapting the diffusive properties for O_2 of the calibration solutions to those of the media to be measured. For example, with different concentrations of solutions of glycerine or KCl diffusion conditions can be attained which resemble those of tissue

In practice, in most cases a 3- or 4-point calibration is sufficient. We use tanks of "extremely pure" nitrogen and oxygen. The calibration gases are two-component mixtures of oxygen and nitrogen produced by a calibrated gas-mixing pump (Type 1 M-100/a-F, Apparatebau H. Wösthoff, D–4630 Bochum). Zero point can also be determined in a saturated Na_2SO_3 solution.

For determination of the calibration curve p_{O_2} versus reduction current, the respective oxygen partial pressure is calculated from the known oxygen concentration of the calibration gas. The following formula is used to calculate the oxygen partial pressure:

$$p_{O_2} = ({}_bp - p_{H_2O}) \times \phi_{O_2}, \tag{6}$$

where p_{O_2} is oxygen partial pressure in kPa (or mmHg); ${}_bp$, temperature-corrected barometer pressure in kPa (or mmHg); p_{H_2O}, water vapor pressure at calibration temperature in kPa (or mmHg); ϕ_{O_2}, volume fraction of oxygen in dry calibration gas (App. B).

Since the slope of the calibration curve can change with time, it is advisable to calibrate the POS before and after each experiment. On an average, the sensitivity of the microcoaxial needle sensor in watery system at 37°C is about 1.2×10^{-11} A kPa^{-1} ($\triangleq 1.6 \times 10^{-12}$ A/mmHg).

Special care is needed to relate the O_2-reduction currents measured in tissue to those of the calibration curves obtained in watery medium. Too thin or defect membranes can produce immense measuring errors if the O_2-diffusion properties of calibration solution and biological media are different. The extent of such errors which might theoretically occur is shown in Fig. 10a. The O_2 reduction current of a bare electrode with circular surface (r_o = 10 μm) at 37°C has been calculated for various media with different diffusion properties. The signal is plotted on the ordinate in dependence on O_2 up to a value of 20 kPA = 150 mmHg on the abscissa. The p_{O_2} signal was calculated as follows:

$$I_1 = 4\, n\, F\, r_o\, S_s\, D_s\, p_{O_2}, \tag{7}$$

where n is the number of elementary charges transported per molecule; F, Faraday constant; r_o, cathode radius; D_s, diffusion coefficient; S_s, solubility coefficient.

Using the different diffusion coefficients reported in the literature (Table 3), we obtain the highest signals in water or diluted electrolytes such as 0.2 mol dm^{-3} NaCl or KCl. This is a finding of practical significance. Assuming, for instance, that with the sensor a p_{O_2} signal of 2 nA is measured in connective tissue, and plotting this value on the calibration curve determined in 0.2 mol dm^{-3} NaCl solution, a p_{O_2} of about 35 mmHg results ($\triangleq$ 4.7 kPa). However, according to the calibration curve calculated by using the proper diffusion coefficient, 2 nA correspond to 112 mmHg ($\triangleq$ 15.0 kPa) in connective tissue. This means that for this particular case, the absolute p_{O_2} determined was too low by a factor of about 3.2. Since it cannot be excluded that the membrane of a sensor has been damaged during an experiment, mistakes can arise. p_{O_2} values determined in the cortex may be too low by a factor of up to approx. 1.4, in the lungs to 1.5, in heart to 1.7, and in muscle to 2.6. These errors cannot be eliminated by intermediate calibration, and hardly by correction factors. The most effective remedy is coordination of the O_2 diffusion properties of the calibration solution with those of the medium to be measured.

Table 3. Coefficients for O_2 diffusion and solubility of various biological media (37°C). The values given in parentheses have not been measured but estimated with the aid of $D_S = P_S/S_S$ and then converted to 37°C according to the dependence on temperature [25]. The corrected values of P_S are: in muscle = 9.73×10^{-12} mol O_2 cm^{-1} s^{-1} atm^{-1} $\triangleq$ 9.59×10^{-14} mol O_2 cm^{-1} s^{-1} kPa^{-1}; in connective tissue = 7.95×10^{-12} mol O_2 cm^{-1} s^{-1} atm^{-1} $\triangleq$ 7.83×10^{-14} mol O_2 cm^{-1} s^{-1} kPa^{-1}. In both cases S_S was assumed to be 8.93×10^{-7} mol O_2 cm^{-3} atm^{-1} = 0.02 cm^3 O_2 cm^{-3} atm^{-1} $\triangleq$ 8.8×10^{-9} mol O_2 cm^{-3} kPa^{-1}

Medium	Diffusion coefficient $D_S \times 10^5 \left[\frac{cm^2}{s}\right]$	Solubility coefficient $S_S \times 10^8 \left[\frac{mol\ O_2}{cm^3\ kPa}\right]$	$\alpha \times 10^2 \left[\frac{cm^3\ O_2}{cm^3\ atm}\right]$	Ref.
Water	2.5	1.06	2.4	[27]
Water	3.3	1.06	2.4	[26]
Serum	2.54	0.94	2.13	[25]
Brain	2.0	0.99	2.25	[74]
Lung tissue	2.3	0.79	1.8	[26]
Heart muscle	1.95	0.93	2.1	[27]
Erythrocytes	1.15	1.11	2.5	[27]
Muscle	(1.09)	–	–	[41]
Connective tissue	(0.89)	–	–	[41]

With exactly defined Pt-cathode surfaces we measured the p_{O_2} signal in water and serum (cf. Chap. II.10) under standardized conditions and compared the values with those calculated. The values were in good agreement, and the values for serum were almost identical. The large scattering range for water shown in Fig. 10a (dotted area) was caused by the different O_2 diffusion coefficients given in the literature. The dotted area is limited by the lowest and highest D_S value.

In other experiments the p_{O_2} signal was measured with bare circular Pt-cathodes (diameter 15 μm) in 0.2% agarose as well as KCl and NaCl solutions of different concentration at 37°C. The result calculated for a 10-μm radius of the cathode shows that the effects of different O_2-diffusion properties of tissue are easily simulated with mixtures of fluids (Fig. 10b).

Another shift of the calibration curve can result when the pH-values of the calibration solution are in the acid range. We observed that the signal increased in the acid milieu and that the N_2 value shifted to higher signals. The N_2 value often increased already by changing pH from about 7.4 to 6.0. When pH further decreased to about 4.0, the N_2 value distinctly increased. As a consequence, when calibrating the POS in an acid medium and using the calibration curve for measurement in neutral or slightly alkaline solutions, the absolute p_{O_2} values become too low. Since physiological NaCl solutions or 0.2 mol dm^{-3} KCl may have acidic pH values under normal calibration conditions, they cannot be used to calibrate needle sensors. It is therefore necessary to adjust the pH of the calibration solution to that of the measuring medium. Such cali-

bration problems are most important with regard to precise polarographic measurements with any kind of electrode systems. They have been discussed by other authors as well [44].

4 Application of p_{O_2} Needle Sensor

Up to now, the microcoaxial needle sensor presented here and some of its modifications have been applied to physiological basic research and used for studies such as

- Estimation of oxygen supply and microcirculation of kidney in vivo and of isolated perfused organs [12, 45].
- Determination of the diffusion coefficients for hydrogen and oxygen in agar-agar-layer and blood as well as in brain and liver homogenates [13, 33].
- Local measurement of p_{O_2} and p_{H_2} in the three bones of the inner ear of guinea-pig and cat under conditions of upper cervical sympathectomy as well as of hemorrhagic hypotension and noise [58, 61].
- p_{O_2} and p_{H_2} clearance in the central nervous system [72].
- Determination of O_2-supply in duck egg to investigate the oxygen partial pressure distribution in albumen, yolk, and embryo in dependence on the breeding period (Lomholt, Baumgärtl, Lübbers, unpubl.).
- Local p_{O_2}-measurement in tissue and the hemolymph of *Tarantula eurypelma* [5, 6].
- Examination of O_2-transport conditions in the pericardium of the crayfish [7].
- Direct determination of diffusion layers in biological systems [42].
- Measurement of oxygen supply and microcirculation in the liver [38, 80].
- Measurement of circulatory disturbance in the hypothalamus of freely moving cats (Betz, Baumgärtl, Reschke, Lübbers, unpubl.).
- Measurement of oxygen consumption in the retina of the crayfish eye (Lues, Baumgärtl, Lübbers, in prep.).
- Measurement of O_2 and H_2 – diffusion in the anterior chamber and vitreous body of the cat eye [17, 18, 64].
- Measurement of p_{O_2} fields and flow-through rates in the carotid body [1–3, 16, 36, 76].
- Estimation of O_2 transport in Walker-tumor in connection with the influence of O_2 supply and p_{O_2} distribution through the cancer inhibitor "ICRF-159" [79].
- Measurement of p_{O_2} profiles for investigation of capillary structure and O_2 regulation in the brain cortex [46, 48, 50].
- Differentiation of flow parameters and O_2 supply to the gray and white matter of the brain [47, 73, 78, 80].

Figure 11 shows an example of p_{O_2}-profiles recorded with needle sensors. The profiles were recorded by continuously advancing the sensor into the rat brain cortex. When the tip of the needle sensor (a) approached the arterial beginning of a capillary, high p_{O_2} values were measured, whilst on other sites p_{O_2} was fairly constant or relatively low. The p_{O_2} measured on the brain surface with a stationary needle sensor (b) was almost constant throughout the experiment. This means that the fluctuations

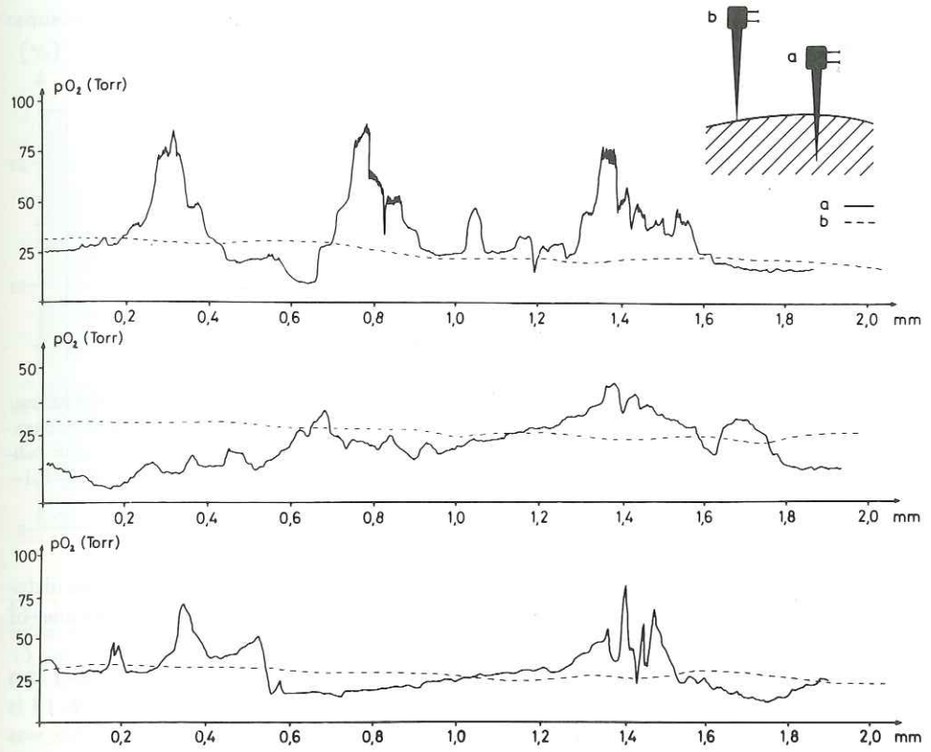

Fig. 11. p_{O_2} profile recorded with a needle sensor vertically inserted into rat cerebral cortex. With continuous speed of 150 μm/min the sensor (*a*) is impaled into the right hemisphere of the exposed cortex at three different points. Apart from arterial p_{O_2} values, a rather steady and relatively low p_{O_2} course is seen at other sites. Throughout the experiment the sensor (*b*) registers the p_{O_2} stationarily on the surface of the cerebral cortex showing a more or less steady course

measured with the sensor (a) were not caused by changes in blood perfusion. The experiment shows quite clearly that oxygen pressure is not uniform in vascularized tissue, but that a p_{O_2} field with different p_{O_2} levels exists.

To estimate reliably the oxygen supply to a tissue, it is useful to investigate the p_{O_2} frequency distribution with the aid of a p_{O_2}-histogram [37, 39, 54, 68], since each stationary situation of oxygen supply has a characteristic p_{O_2} distribution. Figure 12 shows a p_{O_2}-histogram recorded from the gray matter of the brain cortex during normoxia. The figure shows the mean value of seven puncture channels (three animals) measured in a tissue layer of 0.2–2.1 mm over steps of 10 μm each and united to classes of 0.65 kPa $\triangleq$ 5 mmHg (abscissa). The ordinate shows the frequency of the classes. More than half of the p_{O_2} values are in the range of 11–30 mmHg ($\triangleq$ 1.5–4.0 kPa), 15% of values are below 10 mmHg ($\triangleq$ 1.33 kPa). 25% are between 31 and 90 mmHg ($\triangleq$ 4.0–12.0 kPa). To interpret the p_{O_2} histograms exactly, we calculate the mean p_{O_2} value and determine the sites of maximum (module) and median indi-

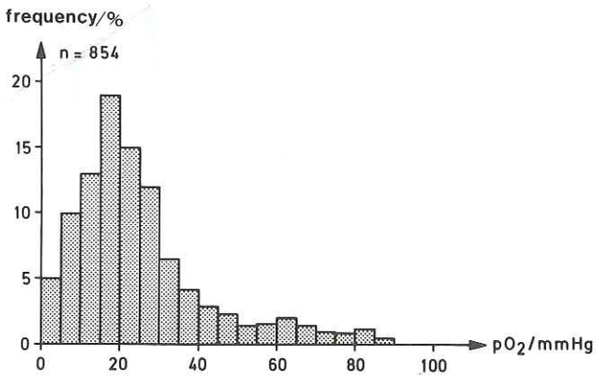

Fig. 12. p_{O_2} histogram of the rat cerebral cortex (depth 0.2–2.1 mm) during normoxia. *Abscissa:* 5 mmHg (0.65 kPa) classes; *ordinate:* percentage frequency (n = 854 out of seven puncture channels, three experiments). Under normal conditions the p_{O_2}-histogram is left-shifted and bell-shaped, characterized by the median (19 mmHg ≙ 2.5 kPa) and modulus (16–20 mmHg ≙ 2.1–2.7 kPa). The mean p_{O_2} = 24.4 mmHg ≙ 3.2 kPa)

cating which values are above or below 50% of the characteristic values. For the histogram shown in Fig. 12 we obtain a mean p_{O_2} of 24.4 mmHg (≙ 3.2 kPa), a median of 19 mmHg (≙ 2.5 kPa) and a module of 16–20 mmHg (≙ 2.1–2.7 kPa).

When plotting the p_{O_2}-differences measured from one 10 μm-step to another in a two-dimensional coordinate system, the p_{O_2} gradient histogram shown in Fig. 13 is obtained. The steepest gradient measured over a length of 10 μm in the rat cortex was 24 mmHg (≙ 3.2 kPa). 34% values do not show a pressure difference over is distance, while about 50% have a p_{O_2} decrease of 1–4 mmHg/10 μm (≙ 0.13–0.53 kPa). According to results of experiments on oxygen supply to tissue, we conclude that oxygen is mainly transported by diffusion.

As well as a carefully prepared sensor, a stable polarization voltage without leaking currents and an exact experimental setup (suitable electrical shielding, stable and sensitive amplifiers) are necessary for reliable p_{O_2} measurements. In some cases, interpretation of the signal is difficult or even misleading because the signal is superimposed by artifacts. To exclude such mistakes, the polarographic setup has to be checked before each experiment by interrupting the measuring circuit by disconnecting the reference electrode for a short time. Whith an adequate measuring arrangement, the signal must immediately decrease to zero when switched on after a short period of polarization, and then return to initial p_{O_2} values.

The damage to tissue through puncturing with needle sensors is one of the main problems. Apart from possible methodological errors arising with the polarographic technique, the fact has to be considered that every puncture causes changes of the physiological milieu of a living object. So far, only very few systematic studies on histologically visible tissue damage have been performed. Together with E. Seidl, we carried out light microscopic investigations to identify the puncture channels in brain preparations. Sensors with an outer diameter of about 3 μm were found to leave channels in the cortex that were marked by vacuolization of the interstitial substance, pyknosis of ganglia cells, and bleeding when vessels were punctured.

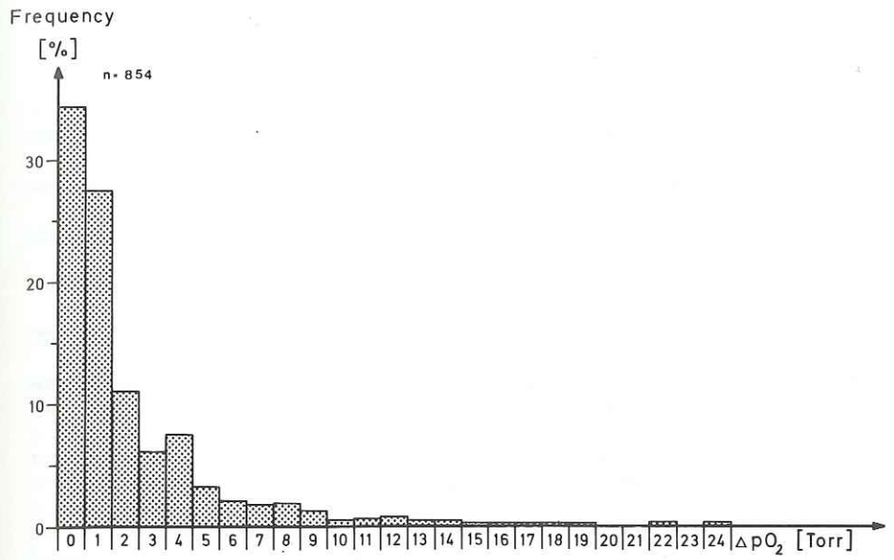

Fig. 13. p_{O_2}-gradients over 10 μm in the gray matter of the rat brain (0.2–2.1 mm). 34% of the values (n = 854) show a steady p_{O_2}. The highest p_{O_2} decrease was 24 mmHg/10 μm ≙ 3.2 kPa/10 μm and was only found twice. 50% of values range between 1 and 4 mmHg/10 μm ≙ 0.13–0.53 kPa/10 μm

In the region of both the sensor tip and lateral shaft, damage to tissue was seen which may influence the experimental results. Damaged tissue was also seen in liver preparations after inserting a simple glass needle sensor (tip diameter about 2 μm) such as used for measurements of ionic activity [66]. In contrast, histological investigation of kidney tissue showed only little damage. In any case, tissue damage is kept at a minimum if the tip diameter of the sensor ranges below 1 μm and if the shaft is very thin. We think that these requirements are satisfactorily fulfilled by the microcoaxial needle sensor developed in our laboratory.

The results of our investigations have shown that micro needle sensors have found broad application to the medico-biological field.

Lately, microelectrodes have also been used for p_{O_2} measurements in marine sediments for ecologico-physiological purposes (Chap. III.2 [35, 62, 63, 71]).

Acknowledgment. The authors wish to thank Mrs. G. Blümel and Mrs. E. Menne for preparing the English translation.

References

1. Acker H (1977) Possible excitation mechanism in the chemoreceptor of the carotid body. Verhandlungsber Ges Lungen- und Atmungsforsch 6:1–13
2. Acker H, Lübbers DW (1976) Oxygen transport capacity of the capillary blood within the carotid body. Pfluegers Arch 366:241–246
3. Acker H, Lübbers DW, Purves MJ (1971) Local oxygen tension field in the glomus caroticum of the cat and its change at changing arterial p_{O_2}. Pfluegers Arch 329:136–155
4. Albanese RA (1973) On microelectrode distortion of tissue oxygen tension. J Theor Biol 38: 143:154
5. Angersbach D (1975) Oxygen pressures in haemolymph and various tissues of the tarantula, *Eurypelma helluo*. J Comp Physiol 98:133-145
6. Angersbach D (1978) Oxygen transport in the blood of the tarantula, *Eurypelma californicum*: p_{O_2} and pH during rest, activity and recovery. J Comp Physiol 123:113–125
7. Angersbach D, Decker H (1978) Oxygen transport in crayfish blood: effect of thermal acclimation and short-term fluctuation related to ventilation and cardiac performance. J Comp Physiol 123:105–112
8. Bartels H, Reinhardt W (1960) Einfache Methode zur Sauerstoffmessung im Blut mit einer kunststoffüberzogenen Platinelektrode. Pfluegers Arch Gesamte Physiol Menschen Tiere 271: 105:114
9. Baumgärtl H (1975) Anwendung der CEAG-SCHIRP-Reinraumtechnik bei der Herstellung von Mikroelektroden zur Aufklärung biologisch wichtiger Reaktionsmechanismen. Staubjournal 17:12–13
10. Baumgärtl H (1978) Nadelelektroden zur Messung der Sauerstoffversorgung, Mikrozirkulation und Ionenaktivität im cellulären Bereich lebender Organismen. Garching Instrumente, München, Analytika
11. Baumgärtl H, Grunewald W, Lübbers DW (1974) Polarographic determination of the oxygen partial pressure field by Pt-microelectrodes using the O_2 field in front of a Pt-macroelectrode as a model. Pfluegers Arch 347:49–61
12. Baumgärtl H, Leichtweiss H-P, Lübbers DW, Weiss Ch, Huland H (1972) The oxygen supply of the dog kidney; measurements of intrarenal p_{O_2}. Microvasc Res 4:247–257
13. Baumgärtl H, Lübbers DW (1973) Platinum needle electrode for polarographic measurement of oxygen and hydrogen. In: Kessler M, Bruley DF, Clark LC Jr, Lübbers DW, Silver IA, Strauss J (eds) Oxygen supply. Urban & Schwarzenberg, München, pp 130–136
14. Baumgärtl H, Lübbers DW (1975) Herstellung von Mikro-p_{O_2}- und p_{H_2}- Elektroden mit der Hochfrequenzkathodenzerstäubungstechnik. Naturwissenschaffen 62:572
15. Bicher HI, Knisely MH (1970) Brain tissue reoxygenation time, demonstrated with a new ultramicro oxygen electrode. J Appl Physiol 28:387–390
16. Bingmann D, Schulze H, Caspers H, Acker H, Keller HP, Lübbers DW (1977) Tissue p_{O_2} in the cat carotid body during respiratory arrest after breathing pure oxygen. In: Acker H, Fidone S, Pallot d, Eyzaguirre C, Lübbers DW, Torrance RW (eds) Chemoreception in the carotid body. Springer, Berlin Heidelberg New York, pp 264–270
17. Briggs D (1972) Experimentelle Untersuchungen zum Sauerstofftransport im Glaskörper des Katzenauges. Dissertation, Marburg
18. Briggs D, Rodenhäuser J-H (1973) Distribution and consumption of oxygen in the vitreous body of cats. In: Kessler M, Bruley DF, Clark LC Jr, Lübbers DW, Silver IA, Strauss J (eds) Oxygen supply. Urban & Schwarzenberg, München, pp 265–269
19. Cater DB (1966) The significance of oxygen tension measurements in tissues. In: Payne JP, Hill DW (eds) Oxygen measurements in blood and tissues and their significance. Churchill, London, pp 155–172
20. Cater DB, Silver IA (1961) Microelectrodes and electrodes used in biology. In: Ives DJG, Janz GJ (eds) Reference electrodes. Academic Press, London New York, pp 464–519
21. Davies PW, Brink F (1942) Microelectrodes for measuring local oxygen tension in animal tissues. Rev Sci Instrum 13:524–533

22. Drenckhahn F-O (1956) Über eine Methode zur Messung des Sauerstoffdruckes im Blut mit der Platin-Kathode. Pfluegers Arch Gesamte Physiol Menschen Tiere 262:169–177
23. Erdmann W, Krell W, Metzger H, Nixdorf I (1970) Ein Verfahren zur Herstellung standardisierter Gold-Mikroelektroden für die p_{O_2}-Messung im Gewebe. Pfluegers Arch 319:R 69
24. Fatt I (1964) An ultramicro oxygen electrode. J Appl Physiol 19:326–329
25. Gertz KH, Loeschcke HH (1954) Bestimmung der Diffusionskoeffizienten von H_2, O_2, N_2 und He in Wasser und Blutserum bei konstant gehaltener Konvektion. Z Naturforsch 96:1–9
26. Grote J (1967) Die Sauerstoffdiffusionskonstanten im Lungengewebe und Wasser und ihre Temperaturabhängigkeit. Pfluegers Arch Gesamte Physiol Menschen Tiere 295:245–254
27. Grote J, Thews G (1962) Die Bedingungen für die Sauerstoffversorgung des Herzmuskelgewebes. Pfluegers Arch 276:142–165
28. Grunewald W (1966) Zur Theorie der Ausgleichsvorgänge an Pt-Elektroden und ihre mathematischen Grundlagen. Dissertation, Marburg
29. Grunewald W (1970) Diffusionsfehler und Eigenverbrauch der Pt-Elektrode bei p_{O_2}-Messungen im steady state. Pfluegers Arch 320:24–44
30. Grunewald W (1971) Einstellzeit der Pt-Elektrode bei Messungen nicht-stationärer O_2-Partialdrucke. Pfluegers Arch 322:109–130
31. Grunewald W (1973) Accuracy and errors of the p_{O_2} measurement by means of the platinum electrode and its calibration in vivo. In: Gross JF, Kaufmann R, Wetterer E (eds) Modern techniques in physiological sciences. Academic Press, London New York, p 309
32. Grunewald W (1973) How "local" is p_{O_2} measurement? In: Kessler M, Bruley DF, Clark LC Jr, Lübbers, DW, Silver IA, Strauss J (eds) Oxygen supply. Urban & Schwarzenberg, München, pp 160–163
33. Grunewald W, Baumgärtl H, Reschke W, Lübbers DW (1967) Bestimmung des H_2-Diffusionskoeffizienten mit der palladinierten Pt-Stichelelektrode zur Messung der Mikrozirkulation im Gehirn. Pfluegers Arch Gesamte Physiol Menschen Tiere 294:R 40
34. Günther H, Aumüller G, Kunke S, Vaupel P (1974) Die Sauerstoffversorgung der Niere. Verteilung der O_2-Drucke in der Rattenniere unter Normalbedingungen. Res Exp Med 163:251–264
35. Jørgensen BB, Revsbech NP, Blackburn TH, Cohen J (1979) Diurnal cycle of oxygen and sulfide microgradients and microbial photosynthesis in a cyanobacterial mot sediment. Appl Environ Microbiol 38:46–58
36. Keller HP, Lübbers DW (1973) Local blood flow measurement in the carotid body of the cat by means of hydrogen clearance. In: Kessler M, Bruley DF, Clark LC Jr, Lübbers DW, Silver IA, Strauss J (eds) Oxygen supply. Urban & Schwarzenberg, München, pp 233–235
37. Kessler M, Bruley DF, Clark LC Jr, Lübbers DW, Silver IA, Strauss J (eds) (1973) Oxygen supply. Urban & Schwarzenberg, München
38. Kessler M, Thermann M, Lang H, Hartel W, Schneider H (1970) O_2-Versorgung lebenswichtiger Organe im Schock unter besonderer Berücksichtigung der Leber. In: Zimmermann W, Staib J (eds) Schock, Stoffwechselveränderungen und Therapie. Schattauer, Stuttgart New York, pp 117–131
39. Kessler M, Höper J, Krumme AB (1976) Monitoring of tissue perfusion and cellular function. Anaesthesiology 45:184–197
40. Kreuzer F, Kimmich H-P (1976) Recent developments in oxygen polarography as applied to physiology. In: Degen H, Balslev I, Brook R (eds) Measurement of oxygen. Elsevier Scientific Publ Comp, Amsterdam Oxford New York, pp 123–158
41. Krogh A (1919) The rate of diffusion of gases through animal tissues with some remarks on the coefficient of invasion. J Physiol 52:391–408
42. Kuhlmann G (1979) Die direkte Bestimmung von Diffusionsschichten an biologischen Systemen mit Mikroelektroden. Diplomarbeit, Bremen
43. Kunze K (1969) Das Sauerstoffdruckfeld im normalen und pathologisch veränderten Muskel. Schriftenreihe Neurologie, Vol III. Springer, Berlin Heidelberg New York
44. Lee YH, Tsao GT (1979) Dissolved oxygen electrodes. In: Ghose TK, Fletcher A, Blakebrough N (eds) Advances in biochemical engineering, vol 13. Springer, Berlin Heidelberg New York, pp 35–86

45. Leichtweiss H-P, Lübbers DW, Weiss Ch, Baumgärtl H, Reschke W (1969) The oxygen supply of the rat kidney: measurements of intrarenal p_{O_2}. Pfluegers Arch 309:328–349
46. Leniger-Follert E (1976) Die Sauerstoffversorgung und die Anpassung der Mikrozirkulation an den Sauerstoffbedarf des Gehirncortex. Habilitationsschrift, Ruhr-Univ Bochum
47. Leniger-Follert E, Lübbers DW (1979) Significance of local tissue p_{O_2} and of extracellular cations of functional and reactive hyperemia of microcirculation in the brain. In: Zülch KJ, Kaufmann W, Hossmann K-A, Hossmann V (eds) Brain and heart infarct, vol II. Springer, Berlin Heidelberg New York, pp 193–201
48. Leniger-Follert E, Wrabetz W, Lübbers DW (1976) Local tissue p_{O_2} and microflow of the brain cortex under varying arterial oxygen pressure. In: Grote J, Reneau D, Thews G (eds) Oxygen transport to tissue, vol II. Plenum Publ Corp, Oxford, pp 361–367
49. Lübbers DW (1966) Methods of measuring oxygen tensions of blood and organ surfaces. In: Payne JP, Hill DW (eds) Oxygen measurements in blood and tissues and their significance. Churchill, London, pp 103–127
50. Lübbers DW (1967) Kritische Sauerstoffversorgung und Mikrozirkulation. In: Wendt CG (ed) Marburger Jahrbuch 1966/67. Elwerth, Marburg, pp 305–319
51. Lübbers DW (1968) The oxygen pressure field of the brain and its significance for the normal and critical oxygen supply of the brain. In: Lübbers DW, Luft UC, Thews G, Witzleb E (eds) Oxygen transport in blood and tissue. Thieme, Stuttgart, pp 124–139
52. Lübbers DW (1969) The meaning of the tissue oxygen distribution curve and its measurement by means of Pt electrodes. In: Kreuzer F (ed) Oxygen pressure recording in gases, fluids, and tissues. Prog Respir Res 3:112–123
53. Lübbers DW (1973) Local tissue p_{O_2}; its measurement and meaning. In: Kessler M, Bruley DF, Clark LC Jr, Lübbers DW, Silver IA, Strauss J (eds) Oxygen supply. Urban & Schwarzenberg, München, pp 151–155
54. Lübbers DW (1977) Bedeutung des lokalen Gewebesauerstoffdrucks und des p_{O_2}-Histogramms für die Beurteilung der Sauerstoffversorgung eines Organs. Prakt Anaesthesiol 12:184–193
55. Lübbers DW (1977) Quantitative measurement and description of oxygen supply to the tissue. In: Jöbsis FF (ed) Oxygen and physiological function. Professional Information Library, Dallas, pp 62–71
56. Lübbers DW, Baumgärtl H (1967) Herstellungstechnik von palladinierten Pt-Stichelelektroden (1–5 μ Außendurchmesser) zur polarographischen Messung des Wasserstoffdruckes für die Bestimmung der Mikrozirkulation. Pfluegers Arch 294:R 39
57. Lübbers DW, Baumgärtl H, Fabel H, Huch A, Kessler M, Kunze K, Riemann H, Seiler D, Schuchhardt S (1969) Principle of construction and application of various platinum electrodes. In: Kreuzer F (ed) Oxygen pressure recording in gases, fluids, and tissues. Prog Respir Res 3: 136–146
58. Maass B (1977) Tierexperimentelle Untersuchungen des sympathischen Einflusses auf die Innenohrfunktion. Habilationsschrift, Düsseldorf
59. Maass B, Baumgärtl H, Lübbers DW (1976) Lokale p_{O_2}- und p_{H_2}-Messungen mit Nadelelektroden zum Studium der Sauerstoffversorgung und Mikrozirkulation des Innenohres. Arch Oto-Rhino-Laryngol 214:109–124
60. Maass B, Baumgärtl H, Lübbers DW (1978) Lokale p_{O_2}- und p_{H_2}-Messungen mit Mikrokoaxialnadelelektroden an der Basalwindung der Katzencochlea nach akuter oberer zervikaler Sympathektomie. Arch Oto-Rhino-Laryngol 221:269–284
61. Maass B, Baumgärtl H, Lübbers DW (1979) Wirkung einer Sympathektomie auf den Sauerstoffpartialdruck (p_{O_2}) in der Cochlea unter hämorrhagischer Hypotension. Laryngol Rhinol 58: 665–670
62. Revsbech NP, Jørgensen BB, Blackburn TH (1980) Oxygen in the seabottom measured with a microelectrode. Science 207:1355–1356
63. Revsbech NP, Sørensen J, Blackburn TH, Lomholt JP (1980) Distribution of oxygen in marine sediments measured with micro-electrodes. Limnol Oceanogr 25:403–411
64. Rodenhäuser J-H, Baumgärtl H, Lübbers DW, Briggs D (1971) Behaviour of the oxygen partial pressure in the vitreous body under various oxygen conditions. In: Proc XXIth Int Congr Ophthalmol. Excerpta Medica Int Congr Ser, No 222, Amsterdam, pp 1624–1628

65. Saito Yukio (1968) A theoretical study on the diffusion current at the stationary electrodes of circular and narrow bond types. Rev Polarogr 15:177–187
66. Schäfer D, Höper J (1976) The influence of glass needle electrodes on rat liver cells and tissue. 6th Eur Congr Electron Microsc, Jerusalem, pp 304–306
67. Schneiderman G, Goldstick TK (1976) Oxygen fields induced by recessed and needle oxygen microelectrodes in homogeneous media. In: Grote J, Reneau D, Thews G (eds) Oxygen transport to tissue, vol II. Plenum Publ Corp, Oxford
68. Schuchhardt S (1971) p_{O_2}-Messung im Myocard des schlagenden Herzens. Pfluegers Arch 322: 83–94
69. Silver IA (1965) Some observations on the cerebral cortex with a ultra-micro, membrane-covered, oxygen electrode. Med Electron Biol Eng 3:377–387
70. Silver IA (1966) The measurement of oxygen tension in tissue. In: Payne JP, Hill DW (eds) Oxygen measurements in blood and tissues and their significance. Churchill, London, pp 135–153
71. Sørensen J, Jørgensen BB, Revsbech NP (1979) A comparison of oxygen, nitrate, and sulfate respiration in coastal marine sediments. Microbiol Ecol 5:105–115
72. Speckmann EJ, Caspers H (1970) Messung des Sauerstoffdruckes mit Platinmikroelektroden im Zentralnervensystem. Pfluegers Arch 318:78–84
73. Stossek K, Lübbers DW (1970) Determination of microflow of the cerebral cortex by means of electrochemically generated hydrogen. In: Russel RW Ross (ed) Brain and blood flow. Pitman Medical and Scientific Publ Co Ltd, London, pp 80–84
74. Thews G (1960) Die Sauerstoffdiffusion im Gehirn. Pfluegers Arch Gesamte Physiol Menschen Tiere 271:197–226
75. Tsacopoulos M, Lehmenkühler A (1977) A double-barrelled Pt-microelectrode for simultaneous measurement of p_{O_2} and bioelectrical activity in excitable tissues. Experientia 33:1337–1338
76. Weigelt H (1975) Der lokale Sauerstoffdruck im *Glomus caroticum* des Kaninchens und seine Bedeutung für die Chemorezeption. Dissertation, Bochum
77. Whalen WJ, Riley J, Nair P (1967) A microelectrode for measuring intracellular p_{O_2}. J Appl Physiol 23:798–801
78. Wrabetz W, Leniger-Follert E, Baumgärtl H, Seidl E, Lübbers DW (1975) Local tissue p_{O_2} in the white matter of cat brain and its regulation. In: Leniger-Follert E, Lübbers DW (eds) Regulation of microcirculation. Arzneimittelforschung (Drug Res) 25:1675
79. Ziegler H (1974) Beeinflussung des lokalen Sauerstoffpartialdruckes im WALKER-Tumor der Ratte durch den Krebshemmstoff ICRF 159. Dissertation, Münster
80. Zorn H (1972) Der Sauerstoffpartialdruck im Hirngewebe und in der Leber bei subtoxischen Kohlenmonoxydkonzentrationen. Staub-Reinhalt Luft 32:151–155